Langmuir

ARTICLE

pubs.acs.org/Langmuir

Investigation into the Reactivity of Unsupported and Supported Ag_7 and Ag_8 Clusters with Toxic Metal Ions

M. S. Bootharaju and T. Pradeep*

DST Unit of Nanoscience (DST UNS), Department of Chemistry, Indian Institute of Technology Madras, Chennai-600 036, India

Supporting Information

ABSTRACT: We report the chemical interactions of unsupported and alumina-supported Ag_7 and Ag_8 clusters protected with MSA (mercaptosuccinic acid) with heavy metal ions Hg(II), Cd(II), and Pb(II) in water at different concentrations. The investigation was carried out to determine the feasibility of this interesting new class of materials called quantum clusters for water purification. These systems were studied using various spectroscopic and microscopic techniques such as ultraviolet−visible spectroscopy, Fourier transform infrared spectroscopy, X-ray diffraction, dynamic light scattering, zeta potential measurements, scanning electron microscopy, transmission electron microscopy, Raman spectroscopy, and photoluminescence spectroscopy and in detail by X-ray photoelectron spectroscopy. We observed that the metal ions interact with both the silver atoms of the clusters and the functional groups of the capping agent (MSA). The mercuric ions were reduced to metallic mercury by both supported and unsupported clusters, due to the feasibility of the redox reaction, whereas no reduction was observed for Cd(II) and Pb(II). As a result of the interaction, the luminescence of the cluster is lost which can be used to sense Hg(II). At lower concentrations, the metal ions were chemically bonded to the carboxylate groups of MSA. Absence of reduction of Hg(II) at lower concentration is due to the chemical affinity of the ligands and the lower silver content per cluster compared to the number of carboxylate groups.

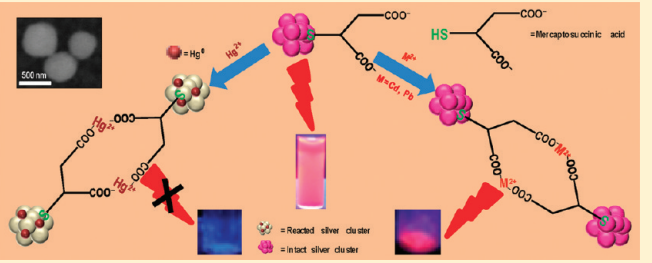

INTRODUCTION

Heavy metal ion contamination of the environment has been a severe problem facing the world for the past several decades. Toxic heavy metals such as mercury, lead, cadmium, etc. can cause adverse damage to many biological systems and can disrupt biological events at the cellular level.[1] According to the environmental protection agency (EPA) guidelines, the allowed levels of lead, mercury, and cadmium in drinking water are 15, 2, and 5 ppb, respectively.[2] The major sources of mercury by natural and anthropogenic origin are oceanic and volcanic eruptions, gold mining, forest fires, and combustion of fossil fuels.[3−5] Mercury in the environment can exist in metallic, inorganic, and organic forms. Metallic mercury vapors and organic mercury derivatives (e.g., methyl mercury) can cause problems in different areas of the brain and many associated activities leading to vision problems, deafness, and loss of sensation and memory.[6,7] Inorganic mercury can cause damage in stomach, heart, kidney, and intestines.[8,9] Mercury is also known to cause the minamata disease.[10,11]

The industrial sources of lead releasing into the environment are battery manufacturing, acid metal plating and finishing, ammunition, tetraethyl lead manufacturing, ceramic and glass industries, printing, painting, and dying.[12] Lead is a potent central neurotoxin and gets accumulated in bones and kidneys, resulting in their damage.[13] Lead causes impairement of physiological functions in humans by occupying the calcium binding sites on numerous calcium-dependent proteins.[14,15] The important sources of cadmium released into the environment by waste streams are electroplating, smelting, alloy manufacturing, and industries associated with pigments, plastic, battery, mining, and refining processes.[16−18] The harmful effects of cadmium include a number of acute and chronic disorders, such as "itai−itai" disease, renal damage, emphysema, hypertension, and testicular atrophy.[19] There are several spectroscopic techniques to detect heavy metal ions such as atomic absorption/emission spectroscopy, inductively coupled plasma mass spectrometry (ICP-MS), and selective cold vapor atomic fluorescence spectrometry, all of which require expensive and sophisticated instrumentation and/or complicated sample preparation processes.[20−22] Simple and naked eye colorimetric detection of these metal ions by metal nanoparticles can overcome these difficulties.[2] In the recent past, noble metal nanoparticles and noble metal clusters have been found to sense heavy metal ions.[23−29]

Noble metal quantum clusters are a class of materials which bridge the gap between nanoparticles and atoms, making this area fascinating. They possess a subnanometer core size with discrete energy levels and exhibit molecule-like[30] properties in their absorption and photoluminescence features. The reactivity of $[Au_{25}(SCH_2CH_2Ph)_{18}]^{-1}$ clusters with metal ions is reported.[31] Many clusters, including $Au_{25}SG_{18}$ (SG-glutathione thiolate) decompose upon the addition of excess Au^{3+}.[32] The reactivity of

Received: March 14, 2011
Revised: May 25, 2011
Published: June 13, 2011

$Au_{15}SG_{12}$ (SG-glutathione thiolate) encapsulated in cyclodextrins with Cu^{2+} has been reported recently.[33] Such clusters are expected to be better systems for metal ion removal as they are expected to be more reactive due to large variation in their reduction potentials. They also have a large fraction of ligands per core metal atom, and these may also be important in metal ion scavenging. We undertook the present study in view of these reasons. It may be pointed out that even nanoparticles exhibit large affinity toward heavy metals, and 4 g of mercury was removed with 1 g of nanoparticles.[34] Noble metal nanoparticles are important for water purification, and a large number of publications exist in this area.[35] In order to make the nanoparticles usable in a flowing water stream, they need to be supported on suitable substrates, and alumina is one good option.

In this paper, concentration-dependent interactions of heavy metal ions with unsupported and alumina-supported silver quantum clusters ($Ag_{7,8}(MSA)_{7,8}$)[36] discovered recently are presented. The as-synthesized cluster is a 80:20 mixture of Ag_8 and Ag_7. These are separated by polyacrylamide gel electrophoresis and characterized by various spectroscopic, microscopic, and mass spectrometric studies.[36] The clusters exhibit well-defined absorption and emission features. In the present experiments, a mixture of the clusters was used as the chemistry of Ag_7 is not likely to be very different from Ag_8 as far as this application was concerned. The interactions were studied at 10, 50, and 100 ppm concentrations of toxic metal ions. At all concentrations of Hg(II), Cd(II), and Pb(II), the chemical interaction of these ions with carboxylate groups of MSA was noticed. In the Hg(II) case alone, reduction to Hg(0) was seen by both the unsupported and supported clusters due to the redox reaction. The luminescence of the cluster is core derived. Due to the involvement of silver atoms in the reduction of Hg(II), the luminescence of the cluster is lost, which can be used for sensing. Above 50 ppm concentrations of Cd(II) and Pb(II), fast precipitation of the clusters was observed.

EXPERIMENTAL SECTION

Materials. In order to keep anion effects the same, acetate salts of the metals were used. Silver nitrate (CDH, India), MSA, methanol, toluene (SRL Chemical Co. Ltd., India), sodium borohydride (Sigma Aldrich), mercuric acetate (Ranbaxy), lead acetate (Rankem), and cadmium acetate (Merck) were purchased from various laboratories and used as such without further purification. Neutral alumina was supplied by SRL, India. The surface area of alumina was 900 ± 50 cm^2/g, and the mean particle size was 0.13 mm.

Synthesis of Ag@MSA Nanoparticles. The clusters were prepared starting from nanoparticles. Ag@MSA nanoparticles were prepared as per the literature.[37] About 448.9 mg of MSA was dissolved in 100 mL of methanol with stirring, at 0 °C. To this, $AgNO_3$ solution (85 mg of $AgNO_3$ in 1.7 mL of distilled water) was added. Then 25 mL of 0.2 M aqueous $NaBH_4$ was added dropwise, and stirring was continued for 1 h. The precipitate of nanoparticles was centrifuged and washed several times with methanol to remove excess sodium borohydride and MSA. Finally, the solvent methanol was evaporated with a rotavapor to get nanoparticles in the powder form.

Synthesis of Silver ($Ag_{7,8}(MSA)_{7,8}$) Clusters. Silver clusters were prepared following interfacial etching in water/toluene biphasic system as per the published literature.[36] MSA was partially dissolved in toluene, and parent Ag@MSA was dissolved in water. An aqueous solution of the as-synthesized Ag@MSA nanoparticles was added to an excess of MSA in toluene. A weight ratio of 1:3 was used (Ag@MSA:MSA). The resulting mixture was stirred for 2 days at room temperature. Initiation of interfacial etching is indicated by the appearance of a blue layer at the interface after 1.0 h. As the reaction proceeds, the color of the aqueous phase changes from reddish brown to yellow and finally to orange. The orange aqueous layer was separated using a separating flask and centrifuged 3−4 times at 10 000 rpm to remove a white precipitate of silver thiolate. Finally the orange aqueous solution was freeze-dried to get a mixture of the clusters. The cluster was washed with excess methanol to remove any traces of silver thiolate and finally dried using rotavapor. This being a mixture of Ag_7 and Ag_8 cluster is designated as $Ag_{7,8}$. The optical absorption and emission of this cluster mixture is dominated by the features of Ag_8.

Preparation of Supported Silver Clusters on Alumina. Silver clusters were supported on neutral alumina by adding 2 mL stock solution of the $Ag_{7,8}$ cluster in aliquots to the calculated amount of alumina and shaking well until the color of the supernatant disappeared. Addition of cluster aliquots was stopped when no fading of color, i.e., no loading, took place. This was monitored by using an UV−vis absorption spectrum of the supernatant also. Thus a saturation point was noticed. This was found to be 0.5 g silver cluster on 100 g of alumina. The aqueous layer was removed and washed with distilled water to remove excess cluster followed by methanol. Finally the loaded cluster was dried using rotavapor to get a powder, and this was denoted as $Ag_{7,8}(MSA)_{7,8}@Al_2O_3$.

Interaction of Silver Clusters and Heavy Metal Ions. For this study, 8.0 mg of silver cluster was mixed with 50 mL of 10, 50, and 100 ppm solutions of Hg(II), Cd(II), and Pb(II) in 100 mL conical flasks and stirred well for 1 day at room temperature and pressure. Here the molar ratios of metal ions to silver in 10, 50, and 100 ppm cases are 0.5, 3.1, and 6.2, respectively. In the case of alumina-loaded cluster, the conditions were the same as in the case of unsupported clusters except that the quantity of the supported clusters was 50 mg.

Instrumentation. UV−vis absorption spectra were recorded with a PerkinElmer Lambda 25 instrument in the range of 200−1100 nm. The FTIR spectra were measured with a PerkinElmer Spectrum One instrument. KBr crystals were used as the matrix for preparing the samples. High resolution transmission electron microscopy (HRTEM) of the samples was carried out using a JEOL 3010 instrument with a UHR pole piece. TEM specimens were prepared by drop-casting one or two drops of aqueous solution to carbon-coated copper grids and allowed to dry at room temperature overnight. All measurements were done at 200 kV to minimize the damage of the sample by the high energy electron beam. Scanning electron microscopy (SEM) images and energy dispersive analysis of X-ray (EDAX) studies were carried out using a FEI QUANTA-200 SEM. For SEM measurements, samples were drop-casted on an indium tin oxide (ITO)-coated conducting glass and dried in ambience. Dynamic light scattering (DLS) and ζ potential measurements were performed with a Zetasizer 3000HSA (Malvern Instruments, U.K.). Photoluminescence measurements were carried out using a HORIBA JOBIN VYON NanoLog fluorescence spectrofluorimeter. Raman spectra were measured using WiTec GmbH confocal micro Raman equipped with a CCD detector. The light source was a Nd:YAG laser of 532 nm wavelength.

X-ray diffraction (XRD) data were obtained with a Shimadzu XD-D1 diffractometer using Cu Kα (λ = 1.54 Å) radiation. The samples were scanned in the 2θ range of 10−90°. X-ray photoelectron spectroscopy (XPS) measurements were done using an Omicron ESCA Probe spectrometer with polychromatic Mg Kα X-rays ($h\nu$ = 1253.6 eV). The X-ray power applied was 300 W. The pass energy was 50 eV for survey scans and 20 eV for specific regions. Sample solution was spotted on a molybdenum sample plate and dried in vacuum. The base pressure of the instrument was 5.0 × 10^{-10} mB. The binding energy was calibrated with respect to the adventious C 1s feature at 285.0 eV. Most of the spectra were deconvoluted to their component peaks, using the software CASA-XPS.

dx.doi.org/10.1021/la200947c |*Langmuir* 2011, 27, 8134–8143

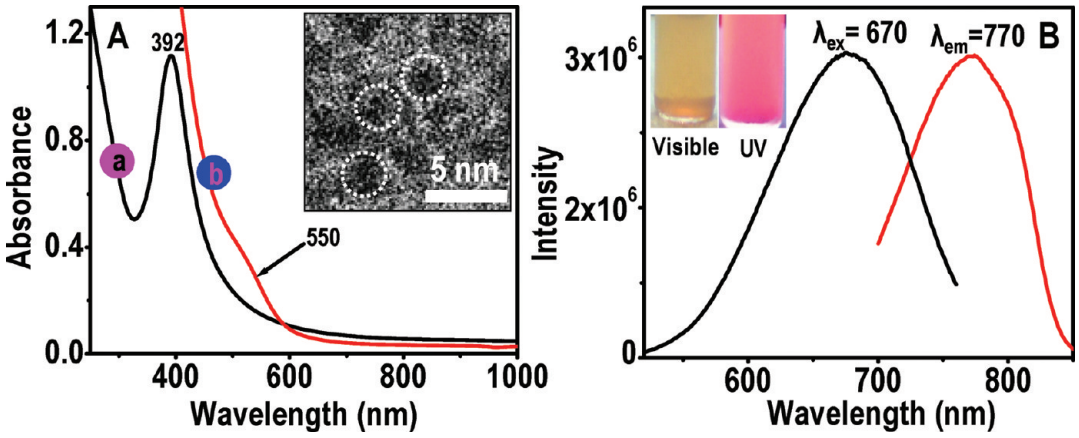

Figure 1. (A) UV−vis absorption spectra of Ag@MSA nanoparticles and $Ag_{7,8}(MSA)_{7,8}$ clusters in water (traces a and b, respectively). Inset of A is the small area TEM image of silver clusters. (B) Photoluminescence spectra of crude $Ag_{7,8}(MSA)_{7,8}$ in water. Black and red traces are the excitation and emission spectra, respectively. The photographs of $Ag_{7,8}(MSA)_{7,8}$ in water−methanol mixture (at 5 °C) are shown as an inset. The yellowish brown solution is under visible light, and the red emission is under a UV lamp.

We have used the suspensions of mixtures for UV−vis and DLS measurements. For TEM and SEM, the precipitated clusters were sonicated for a few minutes and drop-casted on carbon-coated copper grids and ITO conducting glass plates, respectively. For FTIR and XPS, the precipitates were used.

RESULTS AND DISCUSSION

The formation of silver nanoparticles and clusters was characterized by using UV−vis spectroscopy, TEM, photoluminescence spectroscopy, XRD, and XPS techniques. A complete characterization of this material has been reported earlier.[36] We present only the essential data here. The Ag@MSA nanoparticles show an optical absorption feature at 392 nm as shown in Figure 1A (trace a). After interfacial etching of nanoparticles with toluene, the surface plasmon peak at 392 nm disappeared (after 48 h) and a shoulder around 550 nm was noticed (Figure 1A, trace b). The small area TEM image of silver cluster is shown as an inset of Figure 1A in which some of the clusters are noted with dotted circles. Figure 1B shows the photoluminescence spectra of the crude silver clusters in water which show an emission at 770 nm (red trace) when excited at 670 nm (black trace) at 5 °C. The photographs of these silver clusters in water and methanol mixture (at 5 °C) are shown as an inset of Figure 1B. The yellowish brown color (left bottle) is under visible light, and the red emission (right bottle) is under a UV lamp. The TEM images of silver nanoparticles and silver clusters are shown in Figure S1 (Supporting Information, SI) which show an aggregation of clusters due to electron beam irradiation as they are sensitive to electron beam exposure (Figure S1B). The Ag@MSA nanoparticles are stable to electron beam irradiation (Figure S1A). The size of the cluster is less than 1 nm whereas nanoparticles are in the 20−40 nm range.

The X-ray diffraction patterns of Ag@MSA nanoparticles and $Ag_{7,8}(MSA)_{7,8}$ clusters are shown in Figure S2. The peaks are broadened due to smaller size of the particles.[38] The diffraction peaks of silver present in Ag@MSA nanoparticles (trace a) were absent in silver clusters (trace b). This may be due to the absence of long-range order and smaller size of the clusters. The formation of silver clusters is further supported by XPS analysis, and the data are compared with Ag(I)MSA thiolate (Figure 2). The Ag(I)MSA thiolate was prepared by grinding $AgNO_3$ and MSA in a 1:1 molar ratio.[38] The XPS survey spectrum of Ag(I)MSA thiolate is shown in Figure S3 which confirms the presence of sulfur, carbon, oxygen, and silver. The Ag $3d_{5/2}$ peak in the thiolate appears at 367.6 eV due to the Ag(I)[39] state (Figure 2A, trace a), whereas in Ag@MSA nanoparticles and clusters, the Ag $3d_{5/2}$ peak is seen at 368.2 eV corresponding to the Ag(0) state[39] (Figure 2A, traces b and c, respectively). The sulfur from MSA is present at 162.2 eV in Ag(I)MSA thiolate (Figure 2B, trace a). The S 2p feature has been deconvoluted to the $2p_{3/2}$ and $2p_{1/2}$ components. Similarly the S 2p peak is noticed at 162.2 eV in nanoparticles and clusters (Figure 2B, traces b and c, respectively) which confirms the thiolate (RS^-) form.[40] The C 1s peaks at 285.0 and 289.0 eV correspond to aliphatic and carboxylate carbons in Ag(I)MSA thiolate, respectively (Figure 2C, trace a). The presence of carboxylate groups on the nanoparticles and clusters is shown in Figure 2C (traces b and c, respectively). The XPS peaks of C 1s at 285.0 ± 0.2, 286.5 ± 0.2, 288.2 ± 0.2, and 289.6 ± 0.2 eV are attributed to C−C, C−O, O−C−O, and O═C−O carbons, respectively.[41] The XPS data of $Ag_{7,8}(MSA)_{7,8}@Al_2O_3$ sample show silver in the Ag(0) state,[39] sulfur as thiolate,[40] and the carboxylate groups from MSA (traces d in Figure 2A, 2B, and 2C). The Al 2p at 74.6 eV due to alumina[42] support is shown in Figure 2D.

Treatment of Unsupported $Ag_{7,8}(MSA)_{7,8}$ Clusters with Hg(II), Cd(II), and Pb(II). After the addition of different concentrations of Hg(II) to the $Ag_{7,8}(MSA)_{7,8}$ clusters, the solutions were analyzed using UV−vis, FTIR, SEM, EDAX, TEM, DLS, and ζ potential measurements and in detail with XPS. When 100 ppm Hg(II) solution was added to the silver cluster, the brown red color of the cluster disappears immediately and a gray color precipitate was obtained within 3 min. This indicates the high reactivity of the clusters, and the color change indicates the chemical change of the clusters. In the 10 ppm case, no precipitate and no color change of the cluster were observed. UV−vis absorption spectra of these solutions at different times of reaction are shown in Figure S4. In the case of 10 ppm, the cluster absorption at 550 nm got red-shifted to 620 nm (trace b, Figure S4D) after 24 h, which may be due to chemical interaction between cluster and added Hg(II). In the 100 ppm case, the enhancement of background at 5 min of reaction is due to the turbidity in the solution.

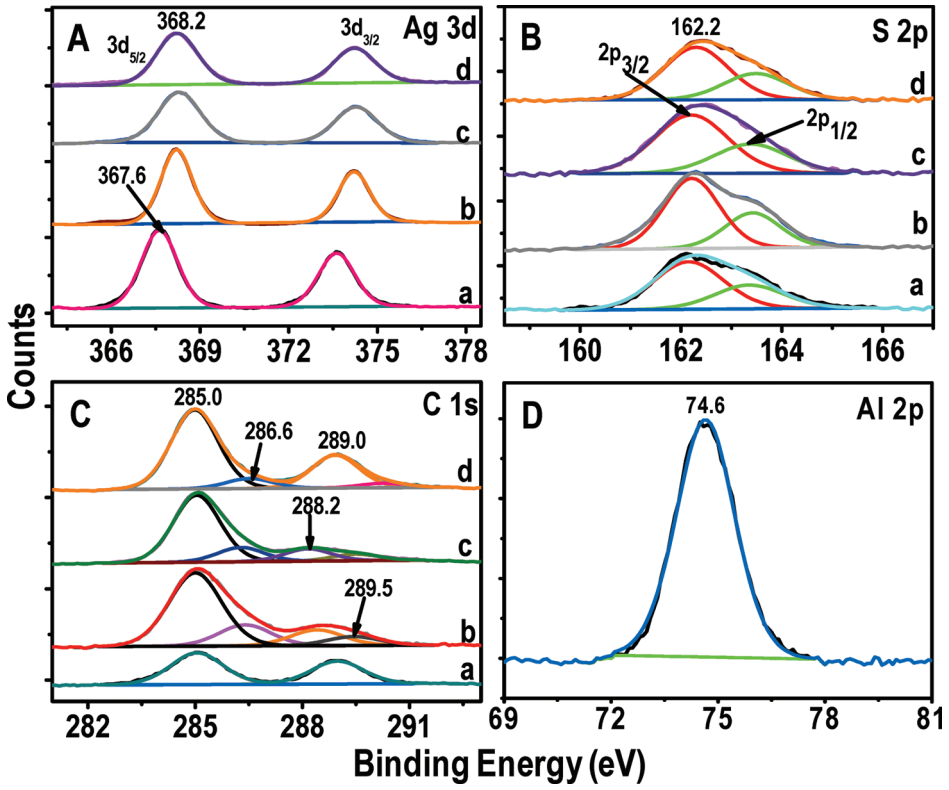

Figure 2. XPS spectra of Ag(I)MSA thiolate (traces a), Ag@MSA nanoparticles (traces b), $Ag_{7,8}(MSA)_{7,8}$ clusters (traces c), and $Ag_{7,8}(MSA)_{7,8}@Al_2O_3$ (traces d) in the Ag 3d, S 2p, and C 1s regions (A, B and C, respectively). The Al 2p region (from alumina support) is shown in D.

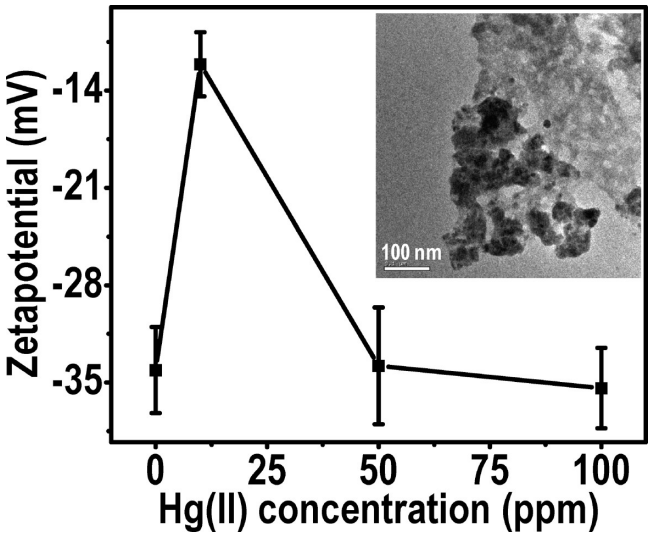

Figure 3. Plot between zeta potentials of solutions of $Ag_{7,8}(MSA)_{7,8}$ clusters treated with 10, 50, and 100 ppm Hg(II) solutions and Hg(II) concentrations. Zero ppm Hg(II) corresponds to parent $Ag_{7,8}(MSA)_{7,8}$ clusters. Inset: TEM image of silver clusters treated with 10 ppm Hg(II).

The absence of cluster feature at 550 nm in 50 and 100 ppm cases (Figures S4A–D) indicates the interaction of Hg(II) with clusters.

The average hydrodynamic diameters of the parent clusters and those treated with 10, 50, and 100 ppm Hg(II) solutions are 20, 7000, 221, and 268 nm, respectively (Figure S5). In the 10 ppm case, it shows that there exist two size ranges centered at 458 and above 7000 nm. In particle number analysis, 38.6% particles have a size of 458 nm and 61.4% particles have a size of 7045 nm. Although there are two peaks in the graph, an average hydrodynamic diameter is reported. The agglomeration of cluster in the 10 ppm case that results in the increase of particle size is supported by the DLS data.[43] As compared to the parent cluster, in 50 and 100 ppm cases, sizes of the particles increased but not as in the 10 ppm case. The reason may be the extensive reaction of silver cluster core with Hg(II) at higher concentrations. The ζ potentials of the parent clusters and clusters treated with 10, 50, and 100 ppm Hg(II) solutions are -34.1 ± 3.1, -12.1 ± 2.3, -33.8 ± 4.2, and -35.4 ± 2.9 mV, respectively (Figure 3). The negative ζ potentials in all the cases indicate the surface negative charge on the cluster due to the carboxylate groups of MSA.[43] In the 10 ppm solution, a large drop of ζ potential ($\sim$20 mV) was observed which may be due to the neutralization of carboxylate negative charge with Hg(II) ions which result in aggregation.[43] This decrease in ζ potential is also supported by decrease of pH of the solution of the cluster from 5.0 to 4.1 due to Hg(II) interaction.[26] The aggregation of cluster was confirmed by TEM images (an image is shown in Figure 3). But in the 50 and 100 ppm cases, the surface charge remains almost unchanged. This may be due to chemical change of Hg(II) to Hg(0) which is supported by XPS.

The interaction of carboxylate groups and Hg(II) was studied using FTIR spectroscopy (Figure S6). The S–H stretching peak at 2548 cm^{-1} present in pure MSA is absent in silver clusters as the binding of MSA occurs in the thiolate form (data are not shown).[43] To show the interaction of Hg(II) with carboxylate groups of MSA, the 1750–1300 cm^{-1} region alone is shown.

dx.doi.org/10.1021/la200947c |*Langmuir* 2011, 27, 8134–8143

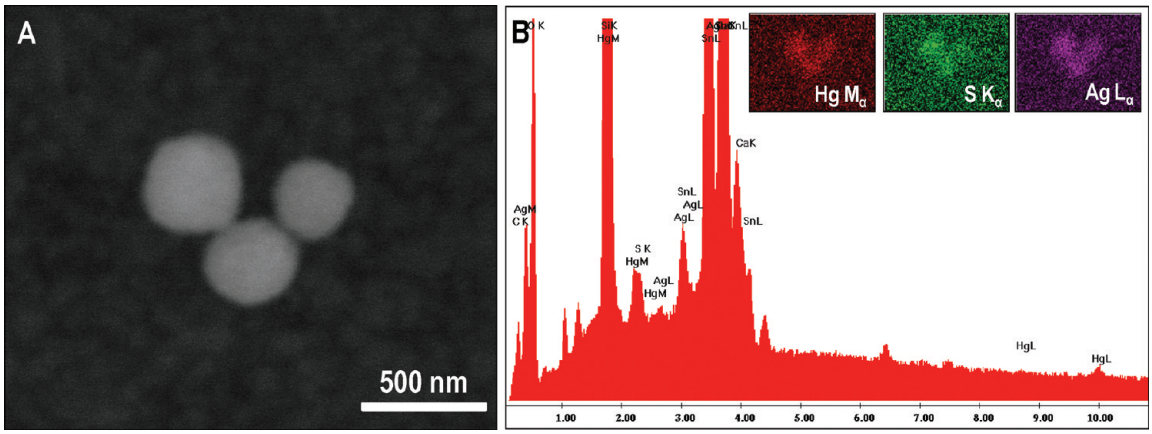

Figure 4. SEM image (A) and EDAX spectrum of silver clusters treated with 100 ppm Hg(II) solution. Inset of B shows the elemental maps of the SEM image (A) showing the presence of Hg, S, and Ag. Si and Sn are due to the substrate used for the SEM measurement.

The IR peak positions of $Ag_{7,8}(MSA)_{7,8}$ clusters are at 1632, 1574, 1404, and 1385 cm^{-1}. The peaks at 1632 and 1574 cm^{-1} are due to carboxylate asymmetric stretching, and those at 1404 and 1385 cm^{-1} are due to carboxylate symmetric stretching modes.[43,44] The differences between these values, $\Delta(\upsilon_{asym}(COO^-) - \upsilon_{sym}(COO^-))$, of 228 and 170 cm^{-1} have been assigned to monodentate and bridging bidentate mode of carboxylates, respectively.[45] After the addition of Hg(II) to the clusters, the peak at 1404 cm^{-1} of the parent clusters got red-shifted to 1399, 1398, and 1397 cm^{-1} in 10, 50, and 100 ppm samples, respectively. These shifts may be due to interaction of Hg(II) with carboxylate groups of MSA.[41,45] In the 10 ppm sample, there is a peak at 1707 cm^{-1} which may be due to −CO− stretching[43] of carboxylate which supports the decrease of ζ potential and aggregation due to Hg(II) interaction with the carboxylate group. In the 100 ppm sample, a new peak appeared at 1375 cm^{-1} which may be due to the carboxylate symmetric stretching mode.[43] The uptake of mercury by silver clusters was studied using SEM, TEM, and XPS techniques. Figure S7 shows the SEM images and EDAX spectrum of the silver clusters treated with 100 ppm Hg(II) solution. The SEM images show the spherical aggregates of the clusters. The EDAX spectrum shows the presence of mercury, silver, and sulfur. The aggregates of these Hg(II) treated clusters were mapped, and the images are shown in Figure 4. Figure 4A is the SEM image. Its corresponding elemental maps (inset) and EDAX spectrum are shown in Figure 4B. These maps confirm the presence of mercury in the aggregated clusters.

Figure S8 shows the TEM and EDAX spectrum of the silver cluster treated with 100 ppm Hg(II) solution. The TEM image shows the aggregates of the clusters clearly, and elemental maps of the same image confirm the presence of silver, sulfur, and mercury on the clusters. The chemistry that happened between the silver clusters and Hg(II) ions at different concentrations was studied using XPS. Figure 5 shows the XPS data of $Ag_{7,8}(MSA)_{7,8}$ clusters treated with different concentrations of Hg(II). Figure 5A is the Hg 4f region. At all concentrations, the Hg $4f_{7/2}$ peaks appeared at 101.1 eV corresponding to Hg(II) bonded to the carboxylate groups of MSA. The peak at 102.6 eV may be due to the complexation of Hg(II) with the more electronegative groups like carboxylates of MSA. The binding energies of Hg $4f_{7/2}$ in Hg(II) and Hg(I) cases are difficult to differentiate.[46] As a result, if partial reduction of Hg(II) to Hg(I) occurs, it cannot be confirmed. At higher Hg(II) concentration (100 ppm), along with Hg(II)/Hg(I) a peak of Hg $4f_{7/2}$ at 100.0 eV was also seen assigned to the Hg(0) state.[47] This reduction of Hg(II) to Hg(0) is possible due to the feasibility of the redox reaction. But at 10 and 50 ppm cases, the metallic mercury peak is not seen. This may be due to the preferential interaction of Hg(II) at lower concentrations with the carboxylate groups of MSA compared to the silver core of the cluster. As Hg(II) reduction is observed in the 100 ppm case, the oxidation of silver is also noticed (Figure 5B). A peak of Ag $3d_{5/2}$ at 367.4 eV is shown in Figure 5B, trace c as in silver oxide.[48] As no reduction of Hg(II) is observed in 10 and 50 ppm cases, the silver is present in the Ag(0) state (Ag $3d_{5/2}$ at 368.4 eV). The Ag(0) state is also present in the 100 ppm sample as all the clusters may not be involved in the reduction of Hg(II). In all the cases, the presence of a monolayer on the silver cluster is observed after treatment with Hg(II). This is confirmed by the presence of S $2p_{3/2}$ at 162.3 eV (Figure 5C) which corresponds to the sulfur bound to silver clusters.[40] Figure 5D shows the C 1s region in which peaks are seen at 285.0, 288.0, and 290.0 eV. The peak at 285.0 eV corresponds to the aliphatic carbon, and those at 288.0 and 290.0 eV are due to the carboxylate carbons in different chemical environments.[41]

Similarly 10, 50, and 100 ppm of Cd(II) solutions were treated with $Ag_{7,8}(MSA)_{7,8}$ clusters. The results are discussed below. When 100 ppm Cd(II) solution was added to the cluster, fast precipitation of the cluster was noticed leaving a colorless supernatant. Similar precipitation was seen in the 50 ppm case also after a few hours. But in the 10 ppm case, no precipitation of clusters and no color change of the cluster solution were noticed. The color of the precipitate in 50 and 100 ppm cases was the same as that of the parent cluster solution (brown red). No color change in all the cases indicates the absence of chemical change for the silver clusters and Cd(II). This is supported by the XPS data also (discussed below).

Time-dependent absorption spectra of silver clusters treated with 50 and 100 ppm Cd(II) solutions show the enhancement in background after 5 min itself, as the interaction is fast (data are not shown). The absorption (at 550 nm) spectrum of the cluster treated with 10 ppm Cd(II) was not changed even after 24 h of treatment. The precipitates obtained in 50 and 100 ppm cases and the 10 ppm solution (in which there is no precipitation) show red emission under a UV light at liquid nitrogen temperature indicating the presence of the cluster. Precipitation may be

dx.doi.org/10.1021/la200947c |*Langmuir* 2011, 27, 8134–8143

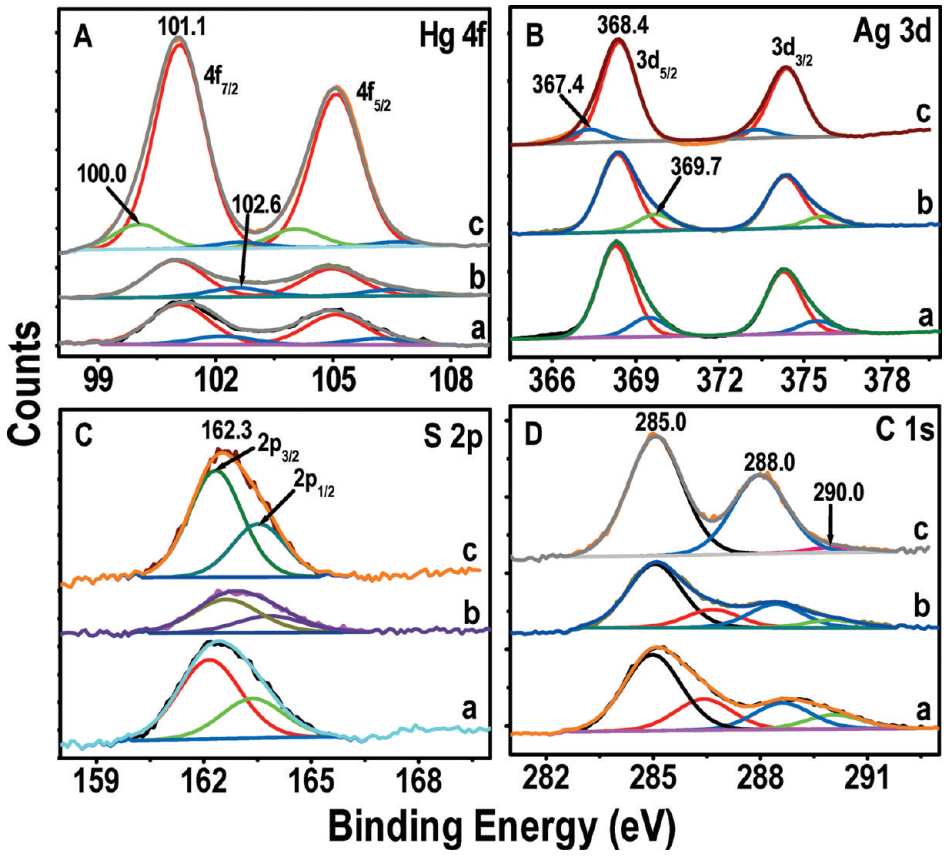

Figure 5. X-ray photoelectron spectra of $Ag_{7,8}(MSA)_{7,8}$ clusters treated with 10, 50, and 100 ppm Hg(II) solutions (traces a, b and c, respectively). Hg 4f, Ag 3d, S 2p, and C 1s regions are shown in A, B, C, and D, respectively.

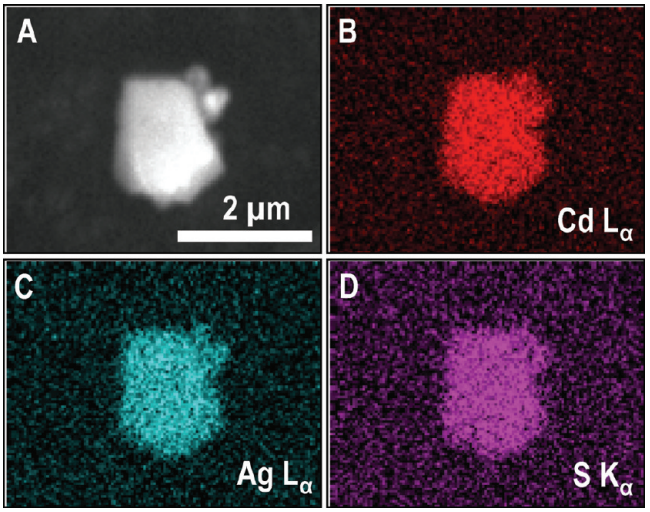

Figure 6. SEM image (A) and elemental maps of Cd, Ag, and S (B, C, and D, respectively) of silver cluster treated with 100 ppm Cd(II) solution.

explained as due to aggregation which also explains the increase in the background in UV−vis spectra. The aggregation of cluster may be due to the chemical interaction of Cd(II) with the carboxylate groups of MSA, supported by FTIR analysis (Figure S9). The asymmetric stretching mode of the carboxylate group at 1574 cm^{-1} in the parent cluster got shifted to 1577, 1568, and 1568 cm^{-1} after treating with 10, 50, and 100 ppm Cd(II) solutions, respectively. The symmetric stretching vibration at 1404 cm^{-1} in the parent cluster got shifted to 1398, 1401, and 1400 cm^{-1} in 10, 50, and 100 ppm samples, respectively. The shift of carboxylate peaks clearly indicates the interaction of Cd(II) with the carboxylate groups of MSA.[49,50] The aggregation of clusters and uptake of cadmium on clusters are analyzed by SEM. Figure 6 shows elemental maps of an aggregate of silver cluster treated with 100 ppm Cd(II) solution. Figure 6A is the SEM image, and Figures 6B−D are the elemental maps of the Cd, Ag, and S, respectively.

Table 1. X-ray Photoelectron Spectroscopic Data of $Ag_{7,8}(MSA)_{7,8}$ Clusters Treated with 10, 50, and 100 ppm Cd(II) Solutions[a]

element core level	binding energy (eV)
Cd $3d_{5/2}$	405.3, 406.7
Ag $3d_{5/2}$	368.4, 369.6
S $2p_{3/2}$	162.4
C 1s	285.0, 286.6, 288.4, 289.0

[a] The results are similar at all concentrations.

The chemistry that happened between silver clusters and Cd(II) at different concentrations was investigated by XPS analysis (Figure S10), and the summarized data are given in Table 1. The results are similar at all concentrations (10, 50, and 100 ppm) of

dx.doi.org/10.1021/la200947c |*Langmuir* 2011, 27, 8134–8143

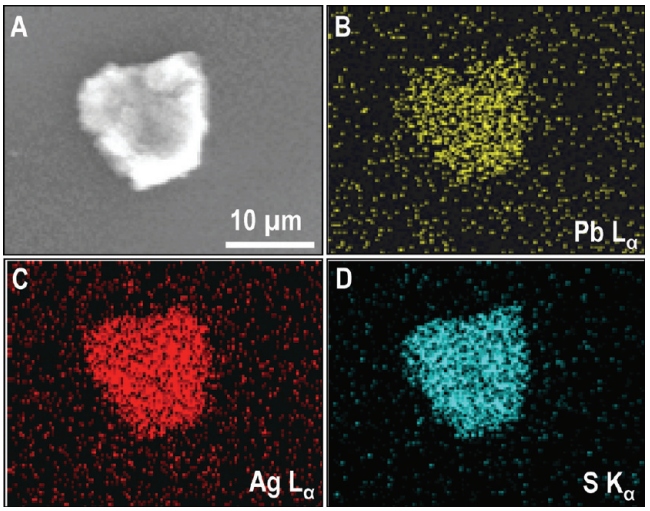

Figure 7. SEM image (A) and elemental maps of Pb, Ag, and S (B, C, and D, respectively) of silver cluster treated with 100 ppm Pb(II) solution.

Cd(II). The peaks of Cd $3d_{5/2}$ were noticed at 405.3 and 406.7 eV. The peak at 405.3 eV is due to cadmium in the +2 state which is bonded with carboxylate groups and at 406.7 eV may be due to the complexation of Cd(II) with carboxylate groups of MSA.[49,50] The data confirm that there is no change in the oxidation state of Cd(II). The Ag $3d_{5/2}$ peak at 368.4 eV is due to Ag(0) from the cluster, and the peak at 369.6 eV may be due to silver in the cluster entity which is in interaction with the metal ion. A peak of S $2p_{3/2}$ is present at 162.4 eV confirming the presence of sulfur bound to the silver cluster core as in the parent cluster.[40] The monolayer protection is intact after the addition of 10, 50, and 100 ppm Cd(II). The C 1s peaks are observed at 285.0, 288.4, and 289.0 eV which are due to aliphatic carbon and carboxylate groups in different chemical environments.[41]

The $Ag_{7,8}(MSA)_{7,8}$ clusters were treated with 10, 50, and 100 ppm solutions of Pb(II). In the 10 ppm solution, the clusters were not precipitated, but in the 100 ppm case, the clusters were precipitated immediately and in the 50 ppm case, precipitation occurred after a few hours. The color of the 10 ppm Pb(II) treated cluster solution and that of the precipitates in the 50 and 100 ppm cases remain the same as that of the parent cluster indicating that no chemical change happened to the cluster. This is supported by the XPS data. The time-dependent absorption spectra of the silver clusters treated with 10, 50, and 100 ppm Pb(II) solutions show large increase in background in the 100 ppm case due to fast precipitation, and this increase continued with time. The silver cluster absorption at 550 nm remained the same with time in the 10 ppm solution (data are not shown). The interaction of silver cluster with Pb(II) was studied using FTIR analysis (Figure S11). The asymmetric stretching of the carboxylate in the parent cluster at 1574 cm^{-1} got shifted to 1552, 1538, and 1538 cm^{-1} in 10, 50, and 100 ppm cases, respectively. Similarly the symmetric stretching of the carboxylate at 1404 cm^{-1} got shifted to 1398, 1396, and 1396 cm^{-1} in these cases, respectively. These shifts indicate the chemical interaction of the carboxylate groups of MSA and Pb(II).[51] Agglomeration of silver clusters was observed in SEM images of the cluster treated with 100 ppm Pb(II). The elemental mapping of an aggregate was done, and the data are shown in Figure 7. Figure 7A shows the SEM image; its elemental maps of Pb, Ag, and S are in Figures 7B, C, and D, respectively. The presence of Pb, Ag, and S indicate the uptake of lead on the silver cluster.

Table 2. X-ray Photoelectron Spectroscopic Data of $Ag_{7,8}(MSA)_{7,8}$ Clusters Treated with 10, 50, and 100 ppm Pb(II) Solutions[a]

element core level	binding energy (eV)
Pb $4f_{7/2}$	138.4, 140.4
Ag $3d_{5/2}$	368.2, 369.3
S $2p_{3/2}$	162.4
C 1s	285.0, 286.5, 288.2, 289.7

[a] The data are similar at all concentrations.

XPS spectra of the silver cluster treated with different concentrations of Pb(II) solutions are shown in Figure S12, and summarized data are given in Table 2. The results are similar at all concentrations of Pb(II). The Pb $4f_{7/2}$ peaks appearing at 138.4 eV are assigned to the +2 oxidation state which may be bonded to the carboxylate groups of MSA.[47] This confirms that no change occurred in the chemical nature of the added Pb(II). Another peak at higher binding energy region (at 140.4 eV) may be due to the complexation of Pb(II) with the carboxylate groups of MSA.[47] A peak of Ag $3d_{5/2}$ at 368.2 eV is seen at all concentrations which corresponds to Ag(0),[39] similar to the parent clusters. Thus no change occurs in the chemical nature of the clusters. Another peak at 369.3 eV was noticed in all cases which may be due to the silver in the cluster which is in interaction with the metal ion. The peak of S $2p_{3/2}$ at 162.4 eV shows sulfur in the bonded state with the silver cluster.[40] After treatment with different concentrations of Pb(II), no change in the MSA monolayer is observed. The C 1s peaks appear at 285.0, 286.5, 288.2, and 289.7 eV. The peak at 285.0 eV is due to aliphatic carbon and other peaks are due to carboxylate carbons in different chemical environments.[41]

Treatment of $Ag_{7,8}(MSA)_{7,8}@Al_2O_3$ Clusters with Hg(II), Cd(II), and Pb(II). Interaction of metal ions at 10, 50, and 100 ppm concentrations with silver clusters loaded on neutral alumina was also studied. As a reference, the uptake of mercuric, lead, and cadmium ions on alumina alone was also studied. In this study, 50 mg of alumina was stirred well for 24 h with 50 mL of 100 ppm metal ion solutions. Thereafter, alumina was analyzed using XPS, and the data corresponding to 100 ppm Hg(II) are shown in Figure S13. The XPS survey spectrum showed only Al and O from alumina with C due to impurities. Figure S13C shows the Hg 4f region in which no Hg $4f_{7/2}$ was seen. This confirms that alumina alone does not adsorb mercury. Similar results were obtained for the Cd(II) and Pb(II) exposed alumina samples also. The Hg(II), Cd(II), and Pb(II) that reacted with alumina loaded with $Ag_{7,8}(MSA)_{7,8}$ were also characterized with FTIR, Raman, and XPS.

The FTIR spectra of $Ag_{7,8}(MSA)_{7,8}@Al_2O_3$ treated with 10, 50, and 100 ppm Hg(II) solutions are shown in Figure S14A. The asymmetric stretching mode of the carboxylate groups at 1582 cm^{-1} in the parent $Ag_{7,8}(MSA)_{7,8}@Al_2O_3$ got shifted to 1570 cm^{-1} at all concentrations (traces b, c, and d). This indicates the binding of Hg(II) with the carboxylate groups of MSA.[41,45] The position of the symmetric stretching mode of the carboxylate groups at 1406 cm^{-1} remains the same before and after treatment of Hg(II). Raman spectra of parent $Ag_{7,8}(MSA)_{7,8}@Al_2O_3$ and the supported clusters treated with Hg(II) are shown in

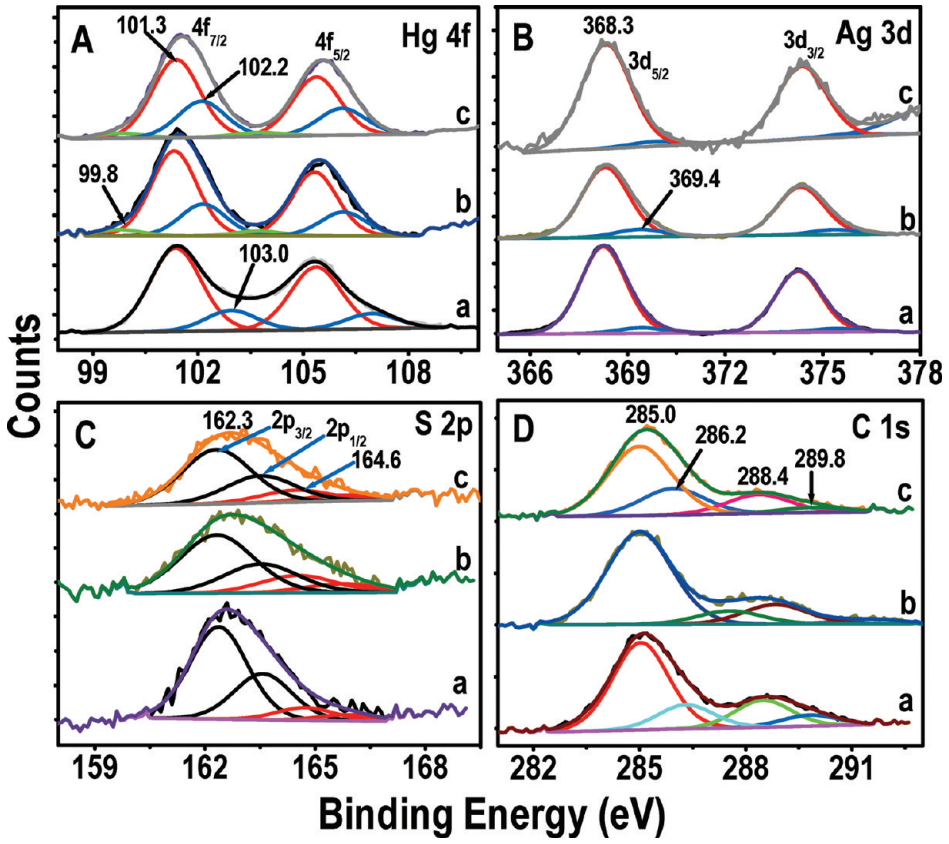

Figure 8. X-ray photoelectron spectra of $Ag_{7,8}(MSA)_{7,8}@Al_2O_3$ clusters treated with 10, 50, and 100 ppm Hg(II) solutions (traces a, b, and c, respectively). Hg 4f, Ag 3d, S 2p, and C 1s regions are shown in A, B, C, and D, respectively.

Figure S14B. In Raman spectral measurements, a 532 nm laser was used for excitation. As the clusters are luminescent, an intense and broad luminescence background is seen. In the 10 ppm sample, luminescence is observed, whereas in 50 and 100 ppm cases, no luminescence background is seen. This suggests that changes occurred in the cluster. It is supported by the photographs (inset of Figure S14B) of the clusters at liquid nitrogen temperature under a UV lamp. The photograph "a" is of the parent $Ag_{7,8}(MSA)_{7,8}@Al_2O_3$ cluster which shows red emission. The 10 ppm sample (b) also shows red emission, whereas 50 and 100 ppm samples did not show the emission (photographs c and d, respectively). The color of the 100 ppm sample became white from the parent yellowish brown powder. The color change may be due to the reduction of Hg(II) by the silver clusters, as confirmed by XPS.

XPS data of the $Ag_{7,8}(MSA)_{7,8}@Al_2O_3$ treated with 10, 50, and 100 ppm Hg(II) are shown in Figure 8. Figure 8A shows the Hg 4f region where a peak of Hg $4f_{7/2}$ at 101.3 eV is observed at all concentrations (traces a, b, and c) which may be due to bonded Hg(II). Other peaks at 103.0 eV (trace a) and 102.2 eV (traces b and c) are also seen which may be due to the complexation of Hg(II)/Hg(I) with the carboxylate groups of MSA. In 50 and 100 ppm cases, a peak at 99.8 eV due to metallic mercury[47] is seen which is formed by the reduction of Hg(II) by silver clusters. But the extent of reduction is relatively less compared to the Hg(II)/Hg(I) states. Figure 8B shows the Ag 3d region where the Ag $3d_{5/2}$ features at 368.3 and 369.4 eV are seen at all concentrations (traces a, b, and c). The former peak corresponds to Ag(0)[39] from the cluster, and the latter is due to the silver in the cluster entity which is in interaction with the metal ion. The rise in intensity around 378.0 eV in Figure 8B, trace c is due to the Hg $4d_{3/2}$ peak. Figure 8C shows the S 2p region in which features at 162.3 and 164.6 eV due to S $2p_{3/2}$ are seen. The former is due to the sulfur bonded to silver cluster, and the latter is due to the formation of disulfides which is relatively small in quantity compared to the bound sulfur.[40] The disulfide formation may also be due to the X-ray induced damage.[52] Figure 8D is the C 1s region where the peaks appear at 285.0, 288.4, and 289.8 eV. The peak at 285.0 eV is due to aliphatic carbon, and other peaks are due to the carboxylate carbons of MSA in different chemical environments[41] which suggests the presence of monolayer protection on the cluster after treatment of Hg(II).

Similarly the $Ag_{7,8}(MSA)_{7,8}@Al_2O_3$ clusters were treated with 10, 50, and 100 ppm Cd(II) and Pb(II) solutions. The colors of the loaded clusters did not change after treatment of Cd(II) and Pb(II). The FTIR spectra after Cd(II) and Pb(II) treatment confirm the chemical interaction of Cd(II) and Pb(II) with the carboxylate groups of MSA. The data are similar to the unsupported cluster−Cd(II)/Pb(II) case (not shown). The XPS data reveal the presence of Cd and Pb in the +2 oxidation state, silver in zero-valent state, and intact monolayer on the cluster which are similar to unsupported cluster−Cd(II)/Pb(II) (data are not shown). The Raman spectra of Cd(II) and Pb(II) treated clusters are shown in Figure S15. In all the cases (10, 50, and 100 ppm) of Cd(II) and Pb(II), the luminescent background was measured indicating the presence of clusters. The photographs of the clusters treated with Cd(II) and Pb(II) are shown as insets of Figures S15A and B which are taken under a UV lamp at liquid

dx.doi.org/10.1021/la200947c |*Langmuir* 2011, 27, 8134–8143

nitrogen temperature. Red emission was seen in all the samples which confirm the unchanged nature of the cluster cores.

The reduction is noticed only in the Hg(II) case, whereas no reduction was seen for Cd(II) and Pb(II). This may be because of the feasibility of the redox reaction at the nanoscale. In aqueous medium, the Ag(I)/Ag redox potential for bulk silver metal is +0.79 V (with respect to NHE), whereas for the silver quantum cluster, its value will decrease due to decrease in particle size.[53] The redox potentials of Hg(II)/Hg, Pb(II)/Pb, and Cd(II)/Cd are +0.8, −0.13, and −0.40 V, respectively (against NHE).[47] The cell emf for the reduction of Hg(II) by silver quantum cluster is positive. The Hg(II) removal capacity of smaller size nanoparticles is more compared to their bigger ones.[54] The silver nanoparticles of 30−40 nm size show reduction of Hg(II) at lower concentrations, and no reduction was noticed at higher concentrations.[47] From these studies, it is clear that the chemical interaction of Hg(II) ions varies with the nanoparticle size and the number of interacting functional groups (attached to the capping agent) per particle. Since clusters contain a large fraction of capping molecules compared to bigger nanoparticles, these can be better candidates for quantitative removal of heavy metal ions from water compared to their nanoparticle analogues.

CONCLUSIONS

The chemical interactions of Hg(II), Cd(II), and Pb(II) with silver core and functional groups of capping molecules were confirmed by several complementary studies. We found that all metal ions (Hg(II), Cd(II), and Pb(II)) interact with the carboxylate groups of MSA of unsupported and alumina-supported $Ag_{7,8}(MSA)_{7,8}$ clusters. Hg(II) is reduced to metallic mercury partially at higher concentrations due to the feasibility of the redox reaction. The reduction of Hg(II) can be seen with the naked eye as the color of the unsupported cluster disappears (giving gray-colored precipitate leaving a colorless supernatant) instantaneously as these clusters are highly reactive with Hg(II). The alumina-loaded silver clusters also show a discharge of color (from yellowish brown to white) due to the reaction with Hg(II). As a result, luminescence of the cluster is lost. Using this reaction, unsupported and alumina-supported silver quantum clusters can be used for Hg(II) sensing. Alumina-loaded silver clusters can be used for quantitative removal of heavy metal ions from contaminated waters. Other metal ions such as Cd(II) and Pb(II) result in fast precipitation of the unsupported clusters at 50 and 100 ppm concentrations.

ASSOCIATED CONTENT

Supporting Information. TEM, XRD, UV−vis, DLS, FTIR, SEM, EDAX, and Raman spectra of unsupported and alumina-supported silver clusters before and after treatment of Hg(II), Cd(II), and Pb(II). This material is available free of charge via the Internet at http://pubs.acs.org.

AUTHOR INFORMATION

Corresponding Author
*E-mail: pradeep@iitm.ac.in.

ACKNOWLEDGMENT

We thank the Department of Science and Technology (DST), Government of India, for constantly supporting our research program on nanomaterials. We thank Dr. Balachandran Unni Nair and Mr. M. Nidhin, CLRI, Chennai, for the DLS measurements. M.S.B. thanks the CSIR for a research fellowship.

REFERENCES

(1) Lee, J. S.; Han, M. S.; Mirkin, C. A. *Angew. Chem., Int. Ed.* **2007**, *46*, 4093–4096.
(2) Kim, Y.; Johnson, R. C.; Hupp, J. T. *Nano Lett.* **2001**, *1*, 165–167.
(3) Eisler, R. *Environ. Geochem. Health* **2003**, *25*, 325–345.
(4) Tchounwou, P. B.; Ayensu, W. K.; Ninashvili, N.; Sutton, D. *Environ. Toxicol.* **2003**, *18*, 149–175.
(5) Wang, Q.; Kim, D.; Dionysiou, D. D.; Sorial, G. A.; Timberlake, D. *Environ. Pollut.* **2004**, *131*, 323–336.
(6) Mutter, J.; Naumann, J.; Schneider, R.; Walach, H.; Haley, B. *Neuroendocrinol. Lett.* **2005**, *26*, 439–446.
(7) Zheng, W.; Aschner, M.; Ghersi-Egea, J. F. *Toxicol. Appl. Pharmacol.* **2003**, *192*, 1–11.
(8) Zalups, R. K. *Pharmacol. Rev.* **2000**, *52*, 113–143.
(9) Vupputuri, S.; Longnecker, M. P.; Daniels, J. L.; Guo, X.; Sandler, D. P. *Environ. Res.* **2005**, *97*, 194–199.
(10) Nolan, E. M.; Lippard, S. J. *Chem. Rev.* **2008**, *108*, 3443–3480.
(11) Chillemi, G.; Mancini, G.; Sanna, N.; Barone, V.; Longa, S. D.; Benfatto, M.; Pavel, N. V.; D'Angelo, P. *J. Am. Chem. Soc.* **2007**, *129*, 5430–5436.
(12) Gupta, V. K.; Agarwal, S.; Saleh, T. A. *J. Hazard. Mater.* **2011**, *185*, 17–23.
(13) Schroeder, H.; Tipton, I. H. *Arch. Environ. Health* **1986**, *17*, 965–978.
(14) Lewis, J. A.; Cohen, S. M. *Inorg. Chem.* **2004**, *43*, 6534–6536.
(15) Bridgewater, B. M.; Parkin, G. *J. Am. Chem. Soc.* **2000**, *122*, 7140–7141.
(16) Holan, Z. R.; Volesky, B.; Prasetyo, I. *Biotechnol. Bioeng.* **1993**, *41*, 819–825.
(17) Volesky, B.; May, H.; Holan, Z. R. *Biotechnol. Bioeng.* **1993**, *41*, 826–829.
(18) Chong, K. H.; Volesky, B. *Biotechnol. Bioeng.* **1995**, *47*, 451–460.
(19) Huang, C. P.; Ostovic, F. B. *J. Environ. Eng. Diu. ASCE* **1978**, *104*, 863–878.
(20) Leermakers, M.; Baeyens, W.; Quevauviller, P.; Horvat, M. *Trends Anal. Chem.* **2005**, *24*, 383–393.
(21) Butler, O. T.; Cook, J. M.; Harrington, C. F.; Hill, S. J.; Rieuwerts, J.; Miles, D. L. *J. Anal. At. Spectrom.* **2006**, *21*, 217–243.
(22) Li, Y.; Chen, C.; Li, B.; Sun, J.; Wang, J.; Gao, Y.; Zhao, Y.; Chai, Z. *J. Anal. At. Spectrom.* **2006**, *21*, 94–96.
(23) Paau, M. C.; Lo, C. K.; Yang, X.; Choi, M. M. F. *J. Phys. Chem. C* **2010**, *114*, 15995–16003.
(24) Huang, C. C.; Chang, H. T. *Anal. Chem.* **2006**, *78*, 8332–8338.
(25) Zheng, Q.; Han, C.; Li, H. *Chem. Commun.* **2010**, *46*, 7337–7339.
(26) Yoosaf, K.; Ipe, B. I.; Suresh, C. H.; Thomas, K. G. *J. Phys. Chem. C* **2007**, *111*, 12839–12847.
(27) Adhikari, B.; Banerjee, A. *Chem. Mater.* **2010**, *22*, 4364–4371.
(28) Lin, Y. H.; Tseng, W. L. *Anal. Chem.* **2010**, *82*, 9194–9200.
(29) Wei, H.; Wang, Z.; Yang, L.; Tian, S.; Hou, C.; Lu, Y. *Analyst* **2010**, *135*, 1406–1410.
(30) Muhammed, M. A. H.; Verma, P. K.; Pal, S. K.; Retnakumari, A.; Koyakutty, M.; Nair, S.; Pradeep, T. *Chem.—Eur. J.* **2010**, *16*, 10103–10112.
(31) Choi, J. P.; Fields-Zinna, C. A.; Stiles, R. L.; Balasubramanian, R.; Douglas, A. D.; Crowe, M. C.; Murray, R. W. *J. Phys. Chem. C* **2010**, *114*, 15890–15896.
(32) Muhammed, M. A. H.; Pradeep, T. *Chem. Phys. Lett.* **2007**, *449*, 186–190.
(33) Shibu, E. S.; Pradeep, T. *Chem. Mater.* **2011**, *23*, 989–999.
(34) Lisha, K. P.; Anshup; Pradeep, T. *Gold Bull. (Geneva)* **2009**, *42*, 144–152.

(35) Pradeep, T.; Anshup. *Thin Solid Films* **2009**, *517*, 6441–6478.
(36) Rao, T. U. B.; Pradeep, T. *Angew. Chem., Int. Ed.* **2010**, *49*, 3925–3929.
(37) Chen, S. H.; Kimura, K. *Chem. Lett.* **1999**, *28*, 1169–1170.
(38) Rao, T. U. B.; Nataraju, B.; Pradeep, T. *J. Am. Chem. Soc.* **2010**, *132*, 16304–16307.
(39) Zhang, H.; Wang, G.; Chen, D.; Lv, X.; Li, J. *Chem. Mater.* **2008**, *20*, 6543–6549.
(40) Ang, T. P.; Chin, W. S. *J. Phys. Chem. B* **2005**, *109*, 22228–22236.
(41) Chen, J. P.; Yang, L. *Langmuir* **2006**, *22*, 8906–8914.
(42) Park, P. W.; Ledford, J. S. *Langmuir* **1996**, *12*, 1794–1799.
(43) Chen, S.; Kimura, K. *Langmuir* **1999**, *15*, 1075–1082.
(44) Alcantara, R.; Lavela, P.; Tirado, J. L.; Stoyanova, R.; Kuzmanova, E.; Zhecheva, E. *Chem. Mater.* **1997**, *9*, 2145–2155.
(45) Wu, N.; Fu, L.; Su, M.; Aslam, M.; Wong, K. C.; Dravid, V. P. *Nano Lett.* **2004**, *4*, 383–386.
(46) Wang, J.; Deng, B.; Chen, H.; Wang, X.; Zheng, J. *Environ. Sci. Technol.* **2009**, *43*, 5223–5228.
(47) Bootharaju, M. S.; Pradeep, T. *J. Phys. Chem. C* **2010**, *114*, 8328–8336.
(48) Shang, L.; Jin, L.; Guo, S.; Zhai, J.; Dong, S. *Langmuir* **2010**, *26*, 6713–6719.
(49) Deng, S.; Ting, Y. P. *Langmuir* **2005**, *21*, 5940–5948.
(50) Crisponi, G.; Diaz, A.; Nurchi, V. M.; Pivetta, T.; Estevez, M. J. T. *Polyhedron* **2002**, *21*, 1319–1327.
(51) Ma, L. J.; Wu, Y. *Anal. Sci.* **2007**, *23*, 799–802.
(52) Esplandiu, M. J.; Noeske, P. L. M. *Appl. Surf. Sci.* **2002**, *199*, 166–182.
(53) Zhang, H.; Li, X.; Chen, G. *J. Mater. Chem.* **2009**, *19*, 8223–8231.
(54) Sumesh, E.; Bootharaju, M. S.; Anshup.; Pradeep, T. *J. Hazard. Mater.* **2011**, *189*, 450–457.